J. Fluid Mech. (1972), *vol.* 51, *part* 3, *pp.* 463–476
Printed in Great Britain

Plasma motions in narrow capillary flow

By J. M. FITZ-GERALD
Department of Mathematics, University of Queensland

(Received 21 March 1971)

Plasma motions in the gaps between successive red cells in narrow-capillary blood flow are obtained in an idealized model, using a series of eigenfunctions to represent the disturbance to a basic Poiseuille flow created by the cells. The flow is matched, in the narrow entry and exit regions, to the lubrication flow in the constricted zone around the red cell (Fitz-Gerald 1969). Basically, the circulating toroidal motion predicted by Prothero & Burton (1961) is obtained in a reference frame in which the cells are considered stationary. Small secondary circulations are also found near the axis and close to the red cells, whose intensity is controlled by the amount of leakback past the cells. Zones of high shear are found along the capillary wall and in some cases on part of the red-cell face; implications of this for mass transport are discussed (see §4). Because of the unusual behaviour of the slowest-decaying dominant eigenfunction circulation and wall shear *increase* as the cell spacing decreases, contrary to expectation, until the spacing becomes very small indeed.

1. Introduction

In previous papers (Fitz-Gerald 1969, 1970) the author considered the problem of the mechanics of red blood cell (RBC) movement through narrow capillaries. Such vessels have diameters comparable with or smaller than that of the RBC, say in the range 3·0 to 8·0 μm (RBC diameter about 8 μm)†; the cells are therefore compelled to travel in single file, with successive cells separated by what Prothero & Burton (1961) termed a 'bolus' of plasma. The flexible RBC's are deformed sufficiently to clear the vessel walls, partly by large-scale pressure forces and viscous drag and partly by local pressure increases in the thin elastohydrodynamic lubrication film around the constriction zone. The importance of this lubrication process was first emphasized by Lighthill (1968, 1969), who pointed out that under negative clearance conditions at least, where cell deformation by lubrication pressure was essential for movement to occur, the resistance to flow of the cell–plasma train would largely be provided by the cells. Furthermore, the exchange of nutrients and metabolites, particularly gases, between tissue and blood would be greatly facilitated in the thin high-shear lubrication zone.

While this is certainly the case in the narrowest capillaries, and in larger ones at low RBC velocity, significant contributions to the resistance, or apparent viscosity, may well be made by plasma in the bolus flow. The amount of plasma

† For references to data concerning diameters, RBC velocities, etc. see, for example, Fitz-Gerald (1972).

leaking back past the RBC is small compared with the total flow so that most of the fluid in the bolus must perform a circulating motion, relative to the red cells, to ensure that the mean plasma velocity be almost equal to the cell velocity. Such a flow may convectively assist the mass transport of slowly diffusing nutrients stored in the plasma, such as fats and proteins.

Previous attempts, both analytic and numerical, to model the bolus flow (Bugliarello & Hsiao 1970; Aroesty & Gross 1970; Bloor 1968; Lee & Fung 1969, 1970) differ significantly amongst themselves; further, very crude boundary conditions were employed. The RBC was assumed in all cases to be a rigid cylinder, either completely occluding the capillary or allowing a simple Couette flow around the wall. In the lubricated flexible red-cell analysis the velocity profiles and fluid leakback were markedly affected by both capillary diameter and RBC velocity; accordingly, it seemed advisable to reconsider the bolus flow problem, to examine the effect of the lubrication flow on the motions in the bolus.

Reynolds numbers for typical capillary flow are very low; mean velocities are of the order of some hundreds of microns/sec, diameters a few microns and plasma kinetic viscosity about two centipoise, giving Re in the range 10^{-2} to 10^{-3}. The detailed geometry of the bolus will therefore probably not greatly affect the flow. Wang & Skalak (1969) found streamline patterns for a line of spheres in a fluid-filled tube which were very similar to those obtained in calculations using plane-ended red cells. Plane-faced cells will also be assumed in the present analysis. These are obtained by truncating the prolate ellipsoids used by Fitz-Gerald (1969) in the lubrication analysis, and the position of the truncation plane is chosen to give a comparatively narrow entry and exit to the bolus, but also to ensure negligible interference with the mechanics of the lubrication flow. This model of the bolus, together with the approximate flow pattern expected, is shown in figure 1.

It should be emphasized that this is a gross simplification of the actual plasma bolus geometry and is chosen to facilitate analysis. *In vivo* and model experiments by Bloch (1962), Brånemark & Lindström (1963), Guest, Bond, Cooper & Derrick (1963), Palmer (1959) and Lee & Fung (1970) have shown that the red cell assumes a variety of shapes in capillaries, depending on capillary size and cell velocity. 'Parachute', 'crepe-suzette' and buckled modes are possible; one feature they have in common is a tendency to an inwards buckling at the trailing edge, presenting a concave surface to the bolus. Fine flow details obtained from the present plane-surfaced truncated ellipsoid model may therefore be inapplicable to actual capillary motion. However, the effects of the leakback from the lubrication zone will still be present regardless of the shape of the red-cell surface; this will be discussed later. In certain unusual blood diseases, haemolytic anaemia and spherocytosis, the geometry used here may be quantitatively quite accurate, but these conditions are comparatively rare.

In the following analysis the ellipsoid is truncated at a point halfway along the semi-major axis. The RBC radius r_c is then $0{\cdot}866a$, where a is the capillary radius, so the requirement of a narrow entry to the bolus is satisfied. Examination of the lubrication solution shows that nearly all the pressure variation and viscous resistance effects occur inside this limit. Small variations of the position of this

truncation point do not significantly affect the velocity profile there, since the lubrication region is well inside this point; neither is the geometry of the bolus greatly altered, since the radius of the red cell is changing only slowly with z there. If h is the lubrication film thickness at the end point (here $0{\cdot}134a$) then the axial velocity profile in the film (Fitz-Gerald 1969) is

$$u(r) = \frac{1}{4\mu}\frac{dp}{dz}\left[r^2 - r_c^2 - \frac{2r_c h + h^2}{\ln(1+h/r_c)}\ln\frac{r}{r_c}\right] - U\frac{\ln(r/r_c)}{\ln(1+h/r_c)}, \tag{1.1}$$

where

$$\frac{dp}{dz} = \frac{aQ - U[(\frac{1}{2}r_c+h)^2 - (2r_c h+h^2)/\ln(1+h/r_c)]}{[(2r_c h+h^2)/16\mu][2r_c^2+2r_c h-(2r_c h+h^2)/\ln(1+h/r_c)]}. \tag{1.2}$$

Here U is the RBC velocity and $2\pi aQ$ the leakback past the cell. These results were obtained in a cylindrical co-ordinate system (r, z) in which the red cells were stationary and the walls moved backwards with velocity $-U$; the same reference frame will be used throughout the present discussion but with the origin re-defined to lie at the mid-point of the centre-line of the bolus.

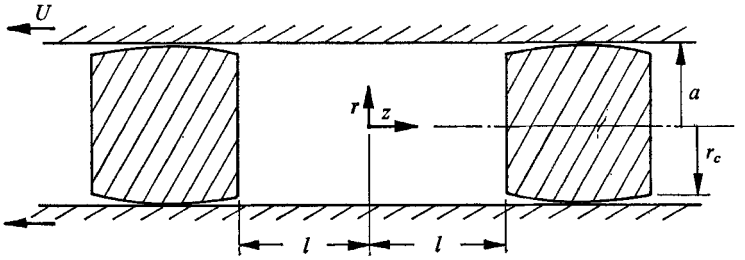

FIGURE 1. Co-ordinate system and dimensions.

The no-slip requirement continues the axial velocity boundary condition on the capillary wall $r = a$ and u must also be zero at the (solid) cell face $0 \leqslant r \leqslant r_c$. The radial velocity will also be taken to be zero on the boundaries; this is clearly true at the capillary wall and red-cell surface, and agrees in the entry gap with a similar assumption made for the lubrication theory. If desired, an approximate radial velocity in the gap could be computed from the continuity equation but this would not satisfy the Navier–Stokes equations. In any case the radial velocities there will be small, and will be ignored in this analysis.

In the next section an analytic solution of this problem is presented in the form of a truncated series of eigenfunctions superimposed on the basic Poiseuille stream function. Results are shown in §4 for several values of the various parameters involved and these are discussed with reference to the mass transport and capillary resistance problems. An exponentially decaying z-dependence is sought for the disturbance functions since it is of interest to discuss the 'zone of influence' of each cell on the plasma flow, in relation to the bolus dimensions. This gives more direct information than the sinusoidal dependence used by Lee & Fung (1969) for their similar problem. The coefficients of the series are obtained using a least-squares technique for minimizing the error in matching the boundary conditions; such an approach seems preferable to the more naive collocation matching used by Lee & Fung and by Zidan (1969) in his solution

(using similar eigenfunctions) for the slow extrusion of a jet of fluid from a nozzle in the spin process for the manufacture of artificial fibres.

An important feature of the flows obtained is the presence of a region of relatively high shear extending along the entire length of the capillary wall, the effect being virtually independent of cell spacing and lubrication film thickness. Interesting also is the intrusion of part of the circulating bolus flow into the entry and exit regions of the lubrication zone, and the continuation, in some cases, of a zone of relatively high shear for some distance up the red-cell face. An unexpected but comparatively unimportant feature is the presence of small slowly moving secondary circulation cells near the axis at the RBC face.

2. General solution for bolus flow

Consider the problem of slow viscous flow of an incompressible fluid, in the absence of body forces, in a circular cylinder of radius a and length $2l$ using axisymmetric cylindrical co-ordinates (r, z) with the origin at the mid-point of the centre-line. Introduce a Stokes stream function ψ, defined by

$$\frac{1}{r}\frac{\partial\psi}{\partial r} = u, \quad -\frac{1}{r}\frac{\partial\psi}{\partial z} = v, \quad \psi(0,z) = 0, \tag{2.1}$$

where u, v are the axial and radial components of the velocity $\mathbf{u}$. In terms of ψ the equation of motion reduces to

$$\left(\frac{\partial^2}{\partial r^2} - \frac{1}{r}\frac{\partial}{\partial r} + \frac{\partial^2}{\partial z^2}\right)^2 \psi = 0. \tag{2.2}$$

Since the cylinder is moving backwards, with velocity $-U$, the boundary conditions at the walls are

$$\left.\begin{aligned} \partial\psi/\partial r &= -aU \quad \text{at} \quad r = a, \\ \psi(a,z) &= aQ \quad \text{if} \quad \psi(0,z) = 0, \end{aligned}\right\} \tag{2.3}$$

where Q is the leakback, assumed known from the lubrication analysis discussed earlier.

At the end of the cylinder general boundary conditions will be allowed, viz.

$$\frac{1}{r}\frac{\partial\psi}{\partial z} = \pm g(r), \quad \frac{1}{r}\frac{\partial\psi}{\partial r} = f(r) \quad \text{at} \quad z = \pm 1. \tag{2.4a}$$

Clearly $u(r, \pm 1) = f(r)$, $v(r, \pm 1) = \pm g(r)$ and the second condition may be replaced by

$$\psi(r, \pm 1) = \int_0^r \rho u(\rho, \pm 1)\, d\rho = F(r), \text{ say.} \tag{2.4b}$$

The only restriction here is that the flow is symmetric about the cross-section $z = 0$. This is prompted by the intended application to capillary flow; anti-symmetric solutions may, of course, be included in an exactly analogous manner, but with a considerable increase in algebraic and computational complexity.

It is convenient to work in non-dimensional terms and new variables are defined as follows.

$$z^* = z/a, \quad r^* = r/a, \quad \psi^* = \psi/(Ua^2), \quad u^* = u/U, \quad f^* = f/U,$$
$$g^* = g/U, \quad F^* = F/(a^2U), \quad G^* = G/aU.$$

Since no confusion can occur the asterisks are omitted for convenience. Equation (2.2) is unchanged and the boundary conditions are now

$$\left.\begin{aligned} \partial\psi/\partial r &= -1, \quad \psi = \tfrac{1}{2}C \quad \text{on} \quad r = 1, \\ \partial\psi/\partial z &= \pm rg(r), \quad \psi = F(r) \quad \text{on} \quad z = \pm\epsilon, \end{aligned}\right\} \tag{2.5}$$

where $C = 2Q/Ua$ and $\epsilon = l/a$. The parameter C was selected to conform with the notation of the lubrication theory.

Because of the non-homogeneous radial boundary conditions (2.5) the system in this form is not Sturm–Liouville. Fortunately, the system can be transformed to one of the Sturm–Liouville type by the change of dependent variable $\psi = \psi_P + \psi_a$, where ψ_P is the (z-independent) Poiseuille solution

$$\psi_P = (\tfrac{1}{2}+c)r^2 - \tfrac{1}{2}(1+c)r^4$$

satisfying (2.2) and the boundary conditions (2.5), and ψ_a is an additional solution, also satisfying (2.2) and homogeneous boundary conditions

$$\psi_a = \partial\psi_a/\partial r = 0 \quad \text{on} \quad r = 1. \tag{2.6}$$

ψ_a is selected to match the boundary conditions on the RBC face and lubrication gap:

$$\left.\begin{aligned} \psi_a &= F(r) - \psi_P = F_1(r) \\ \partial\psi_a/\partial r &= \pm rg(r) = G(r) \end{aligned}\right\} \quad \text{on} \quad z = \pm\epsilon. \tag{2.7a,b}$$

The perturbing solution ψ_a may conveniently be obtained as a series of separated eigensolutions of (2.2), which may be written as

$$\left(L + \frac{\partial^2}{\partial z^2}\right)^2 \psi = 0 \quad \text{where} \quad L \equiv \frac{\partial^2}{\partial r^2} - \frac{1}{r}\frac{\partial}{\partial r}.$$

Explicitly this is

$$L^2\psi + 2\left(L\frac{\partial^2}{\partial z^2}\right)\psi + \frac{\partial^4}{\partial z^4}\psi = 0. \tag{2.8}$$

Separated solutions may be obtained by requiring that either

$$\partial^2\psi/\partial z^2 = \alpha^2\psi \tag{2.9}$$

or

$$L\psi = \beta^2\psi. \tag{2.10}$$

Real values of the separation constant α or β are selected to give solutions with exponential decay, away from the site of disturbance, to the basic Poiseuille flow. This gives more direct information on the degree of interference of disturbances from successive red cells, as the bolus length varies, than does the sinusoidal z-dependence chosen by Lee & Fung (1969, 1970). Equation (2.9) gives rise to a solution of (2.8) of the form

$$A\,\mathrm{e}^{\pm\alpha z}r^2J_0(\alpha r) + B\,\mathrm{e}^{\pm\alpha z}rJ_1(\alpha r), \tag{2.11}$$

while (2.10) gives solutions

$$(A + Bz)\,\mathrm{e}^{\pm\beta z}rJ_1(\beta r). \tag{2.12}$$

Clearly solutions of the form (2.12) cannot satisfy both of the conditions of (2.6) and will thus be ignored. Application to (2.11) of the boundary conditions (2.6), which are satisfied by each separated solution separately, gives simultaneous linear equations for A and B,

$$\begin{pmatrix} J_0(\alpha) & J_1(\alpha) \\ 2J_0(\alpha)-J_1(\alpha) & J_0(\alpha) \end{pmatrix} \begin{pmatrix} A \\ B \end{pmatrix} = \begin{pmatrix} 0 \\ 0 \end{pmatrix}, \tag{2.13}$$

which have non-trivial solutions only if

$$\alpha[J_0^2(\alpha)+J_1^2(\alpha)] = 2J_0(\alpha)J_1(\alpha). \tag{2.14}$$

Solutions of (2.14) form a set (α_n) of discrete eigenvalues for the separation constant α. They are all complex and those of large modulus (large n) may be shown to have the asymptotic form $\alpha_n \sim \frac{1}{2}(2n+1)\pi \pm i \ln(4n+2)\pi$. The first few eigenvalues are given in table 1. Scarton (1970) has shown in a study of periodic compressible viscous flow in a tube that two bands of eigenvalues exist. In the limit of zero frequency these reduce to the complex conjugate pairs obtained here. The eigenvalue $\alpha_0 = 0$ is degenerate and bifurcates for non-zero frequency (Scarton 1970; Scarton & Rouleau 1971*a*, *b*). In the present case the corresponding eigensolution satisfying $\psi = 0$ on the wall is the Poiseuille one $A(r^2-r^4)$, which can only satisfy the zero velocity condition on the wall if $A = 0$. This solution will therefore be ignored in the present analysis.

0	Re (α_n)	$\pm$ Im (α_n)
0	0	0
1	4·466299	1·467470
2	7·694104	1·726971
3	10·874574	1·894943
4	14·038891	2·020063
5	17·195565	2·119946
6	20·347968	2·203124
7	23·497724	2·274406
8	26·645717	2·336779
9	29·792475	2·392226
10	32·938331	2·442135

TABLE 1

Corresponding eigensolutions even in z are of the form

$$\chi_n(r,z) = \frac{\cosh(\alpha_n z)}{\cosh(\alpha_n \epsilon)}[r^2 J_0(\alpha_n r) - S_n r J_1(\alpha_n r)] \tag{2.15}$$

(ignoring the singular Bessel functions of the second kind), where

$$S_n = J_0(\alpha_n)/J_1(\alpha_n)$$

and χ_n is defined so that at $z = \pm\epsilon$

$$\chi_n(r, \pm\epsilon) = \psi_n(r) = r^2 J_0(\alpha_n r) - S_n r J_1(\alpha_n r). \tag{2.16}$$

The differential equation and boundary conditions are real, hence ψ_a must be real. Further, since the eigensolutions occur in conjugate pairs χ_n, $\overline{\chi}_n$ (where χ_n

corresponds to the nth eigenvalue in the first quadrant) ψ_a may be written as

$$\psi_a = \tfrac{1}{2}\sum_1^\infty (B_n\chi_n + \bar{B}_n\bar{\chi}_n)$$

$$= \mathrm{Re}\sum_1^\infty B_n\chi_n. \tag{2.17}$$

At $z = \epsilon$ this may be written

$$\psi_a(r,\epsilon) = \sum_1^\infty B_n^R\psi_n^R - \sum_1^\infty B_n^I\psi_n^I, \tag{2.18}$$

where $\psi_n = \psi_n^R + i\psi_n^I$ and $B_n = B_n^R + iB_n^I$. It seems plausible, although difficult to prove, that both $\{\psi_n^R\}$ and $\{\psi_n^I\}$ constitute complete sets over the function space satisfying (2.6). All relevant eigenvalues have been obtained, so that no other eigensolution, having a different z-dependence, is possible.

The radial velocity at $z = \epsilon$ corresponding to any eigenfunction is given by

$$v(r,\epsilon) = \frac{1}{r}\frac{\partial\chi_n}{\partial z}\bigg|_{z=\epsilon} = -\alpha_n\frac{\psi_n}{r}\tanh(\epsilon\alpha_n).$$

Writing $\alpha_n\tanh(\epsilon\alpha_n) = a_n + ib_n$, the radial velocity at $z = \epsilon$ for the solution (2.18) is obtained from

$$\frac{\partial\psi_a}{\partial z}\bigg|_{z=\epsilon} = \Sigma B_n^R(a_n\psi_n^R - b_n\psi_n^I) - \Sigma B_n^I(a_n\psi_n^I + b_n\psi_n^R). \tag{2.19}$$

Truncations of the series (2.17) or (2.18) are now used to match the prescribed functions in (2.7). A simultaneous least-square error fit is obtained. Define $\mathscr{I}$ to be the integral

$$\int_0^1 \omega(r)\left[\left\{F_1(r) - \sum_1^N B_n^R\psi_n^R + \sum_1^N B_n^I\psi_n^I\right\}^2 + \left\{G(r) - \sum_1^n B_n^R(a_n\psi_n^R - b_n\psi_n^I) + \sum_1^N B_n^I(a_n\psi_n^I + b_n\psi_n^R)\right\}^2\right]dr,$$

where N is the number of terms in the truncated series and $\omega(r)$ is a convenient weighting function, then $\{B_n^R\}$, $\{B_n^I\}$ may be obtained as solutions of the $2N$ equations

$$\partial\mathscr{I}/\partial B_n^R = 0, \quad \partial\mathscr{I}/\partial B_n^I = 0 \quad (n = 1, \ldots, N), \tag{2.20}$$

which are derived explicitly in appendix A.

Examination of the form of the eigenfunctions suggests that $\omega(r) = r^{-1}$ is a suitable weighting function. This makes the integrals

$$\int_0^1 \omega(r)\psi_n^R\psi_m^R dr, \quad \int_0^1 \omega(r)\psi_n^R\psi_m^I dr, \quad \int_0^1 \omega(r)\psi_n^I\psi_m^I dr$$

decrease rapidly as $(n-m)$ increases from zero, giving a matrix for the equations which is strongly diagonally dominated (i.e. well-conditioned). This is of importance when error propagation in the numerical solution of (2.19) is being considered. An outline of the argument used to arrive at this form for $\omega(r)$ is given in appendix C.

For the plasma flow described in § 1 the functions $F(r)$, $g(r)$ take special forms

obtained from (1.1) and (1.2), in appropriate non-dimensional variables. Numerical details of the procedure are given in appendix B. It should be noted that although this solution was developed primarily to examine the case of flow in narrow capillaries, eigenfunctions expansions similar to those developed here may be used to solve problems such as viscous entry flow in a pipe at Reynolds number $\ll 1$ and the flow of gases in a simplified model of the terminal bronchioles and alveolar ducts of the lung (Davidson & Fitz-Gerald 1972).

3. Results

Before discussing particular solutions of the plasma flow problem it is of interest to examine the properties of the eigenfunctions. Streamlines for the real and imaginary parts of χ_1 and χ_2 are shown in figures 2(*a*)–(*d*) for $\epsilon = 1$. As expected, the functions tend to decrease from $z = \epsilon$ to $z = 0$, the rate of decay increasing as the order of the eigenfunction increases. However, for a given r the functions need not exhibit monotone decay and local increases may occur. In the case of χ_1^R this effect is so marked that the maximum value of the function occurs off the line $z = \epsilon$. The behaviour of χ_1^R as ϵ decreases is illustrated in figures 2(*e*)–(*h*); similar plots for χ_1^I are given for comparison. The maximum value achieved by χ_1^R actually increases as ϵ decreases and for $\epsilon = 0{\cdot}2$ this maximum occurs at $z = 0$. Over most of the region, therefore, χ_1^R increases markedly, rather than decreasing from $z = \epsilon$ to $z = 0$. This somewhat unexpected feature of the first eigenfunction has important consequences for the flow patterns in inter-erythrocyte plasma spaces.

Figure 3 shows streamlines for flow corresponding to a fairly small value of the leakback parameter, $C = 0{\cdot}025$, and three values of ϵ; this value of C corresponds to a comparatively close-fitting high-resistance red-cell fit. There are several noteworthy features. First, there is a region of high shear near the capillary wall, extending the length of the plasma bolus, and continuing into the lubrication zone. This region is comparatively unaffected by variations in ϵ; similar calculations with $C = 0{\cdot}05$ show that leakback (related closely to film thickness) in the lubrication zone also has little influence on the high-shear wall region.

There is, in some cases, a second high-shear region on the outer parts of the red-cell face. Unlike that on the capillary wall, this is very dependent on ϵ, increasing in intensity as ϵ decreases. The maximum value taken by the stream function also increases as ϵ decreases. This is due to the anomalous behaviour of the real part of the first eigenfunction, which is the dominant member of the series, particularly for small ϵ. Ultimately, of course, as ϵ becomes very small and the eigenfunctions vary little in the region of the flow, the shear and stream function values decrease again and tend to zero with ϵ (except near the capillary wall).

The unexpected form of the streamlines for $\epsilon = 1{\cdot}0$, with a 'necking' of the main circulation and a secondary circulation near the middle of the red-cell face, seems to be dependent on the amount of leakback through the lubrication zone. Figure 4 shows streamlines for $\epsilon = 1{\cdot}0$, $c = 0{\cdot}05$; here there is much less disturbance from the simple toroidal circulation found by Aroesty & Gross (1970), Bugliarello & Hsaio (1970) and Bloor (1968) for the fixed-leakback rigid-cell model.

As mentioned earlier, it is possible that variations of bolus geometry may influence details of the flow. However, in this case it appears that the secondary circulation is mainly a function of the type of lubrication flow experienced by the red cell, in particular of the gap thickness parameter C. For completeness a schematic

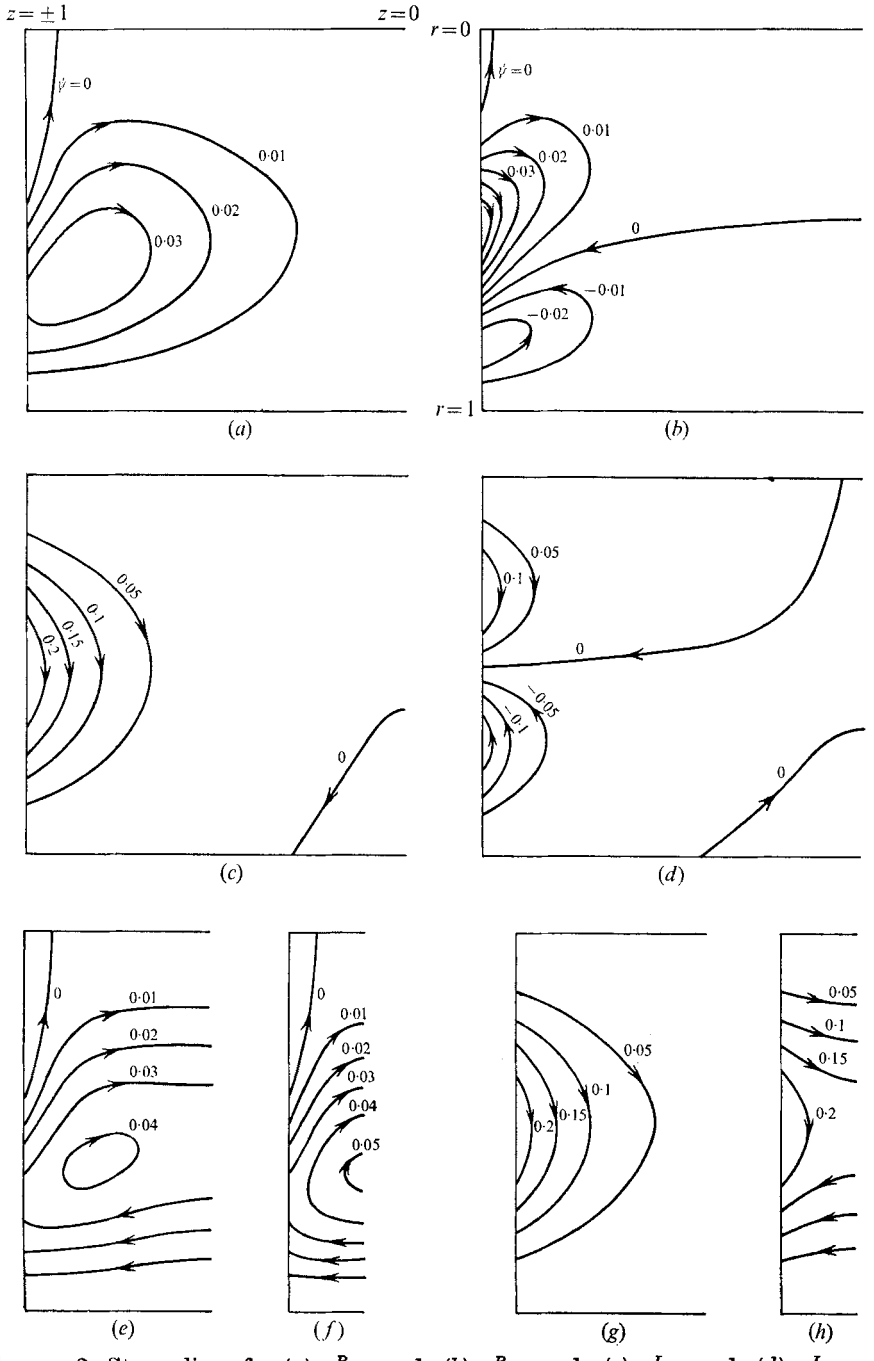

FIGURE 2. Streamlines for (*a*) χ_1^R, $\epsilon = 1$, (*b*) χ_2^R, $\epsilon = 1$, (*c*) χ_1^I, $\epsilon = 1$, (*d*) χ_2^I, $\epsilon = 1$, (*e*) χ_1^R, $\epsilon = 0{\cdot}5$, (*f*) χ_1^R, $\epsilon = 0{\cdot}2$, (*g*) χ_1^I, $\epsilon = 0{\cdot}5$, (*h*) χ_1^I, $\epsilon = 0{\cdot}2$.

diagram of the streamline patterns around the entry to the lubrication zone is shown in figure 5 and in figure 6 streamlines for the flows of figure 3 are plotted in a co-ordinate system fixed relative to the capillary, rather than the red cells.

A final remark concerns the dependence of the pressure drop in the plasma bolus on ϵ. Lee & Fung (1970), Bugliarello & Hsaio (1970) and Bloor (1968) all find that the pressure gradient in the plasma bolus increases as ϵ decreases and does so rapidly for ϵ less than about 0·5; similar experimental findings were

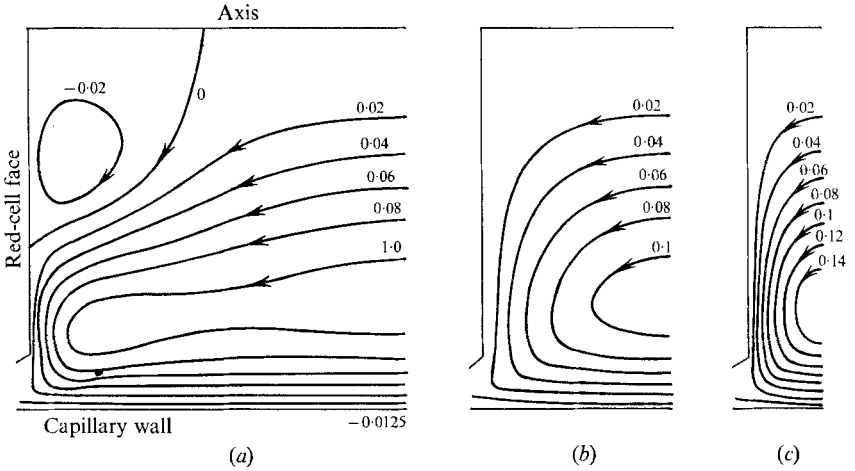

FIGURE 3. Streamlines for the bolus flow, $C = 0{\cdot}025$, $\epsilon = 1{\cdot}0$, $0{\cdot}5$, $0{\cdot}2$ for (*a*), (*b*), (*c*) respectively.

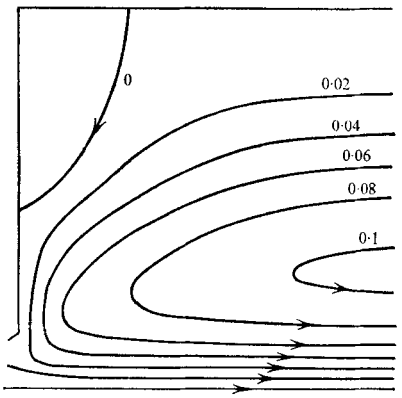

FIGURE 4. Streamlines for bolus flow, $C = 0{\cdot}05$, $\epsilon = 1{\cdot}0$.

reported by Prothero & Burton (1962). These results are confirmed by the increase in shear rates as ϵ decreases found in this analysis. However, the important quantity, as far as the resistance to motion in the plasma spaces is concerned, is the total pressure drop over the length of capillary occupied by plasma and how this depends on cell-spacing variations. Numerical difficulties in evaluating derivatives of the series solutions used here unfortunately prevent relevant information being obtained; the derived series did not, in fact, converge. More work on this problem seems to be indicated to resolve the conflict of other solutions mentioned above.

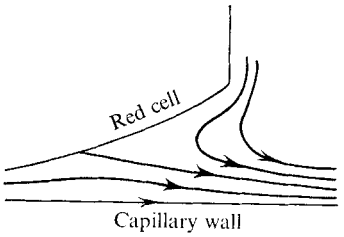

FIGURE 5. Schematic view of streamlines around the entrance to the lubrication region.

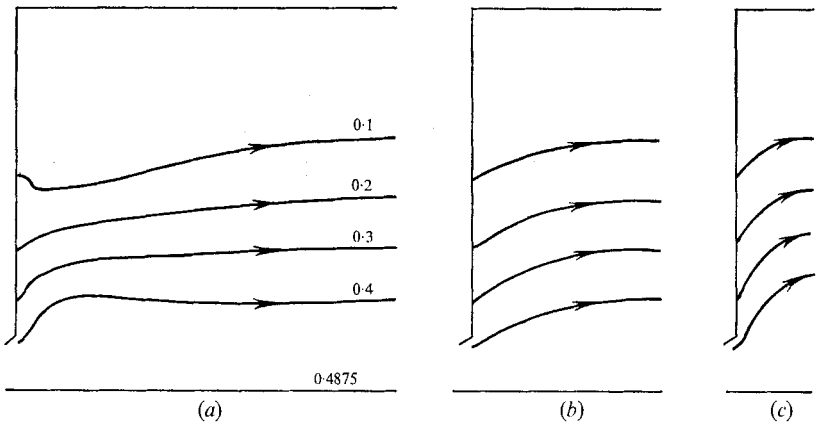

FIGURE 6. Bolus flow streamlines in co-ordinate system fixed relative to the capillary, $C = 0{\cdot}025$, $\epsilon = 1{\cdot}0, 0{\cdot}5, 0{\cdot}2$ for (*a*), (*b*), (*c*) respectively.

4. Implications for mass transport

The relevance of these flow patterns to mass transport depends on the Péclet number for any particular molecular species. In narrow capillaries typical velocities are of order 100–1000 μm/sec and diameters are 3–8 μm. The kinematic diffusivity for oxygen in plasma may be estimated to be $1{\cdot}5 \times 10^{-5}$ cm^2/sec (Landis & Pappenheimer 1963). For oxygen, therefore, Péclet numbers are of order unity ($0{\cdot}35 < Pe < 7$ for the values given) and convection might be expected to be at least as important as diffusion for mass transfer. Numerical studies by Aroesty & Gross (1970), however, show that convective effects are negligible for Pe less than about 10 but it should be noted that these calculations were for a completely occluded capillary. Plasma emerging from the thin lubrication zone will be well supplied with oxygen since a large proportion of transfer will occur across the constricted region where diffusion paths are shortest. This oxygen-charged plasma will continue to supply oxygen to the surrounding tissue in the high-shear zone of the bolus near the capillary wall. There may be additional enhancement of transfer due to the high-shear regions on the red-cell face.

Péclet numbers for proteins such as albumin lie in the range 10–100; convection will therefore be of considerable importance in controlling the supply to tissue of such a high molecular weight and slowly diffusing species. Moreover, the available protein contained in blood is stored principally in the plasma, rather

than the cell so rotation of the inner bolus, bringing large proportions of plasma adjacent to the high shear layer on the capillary wall, will ensure that diffusion path lengths for protein are minimized. In this context it is interesting to note that recent theories (discussed, e.g. by Luft, 1966) of mechanisms of transport of lipid-insoluble molecules such as protein across the endothelium (wall) consider that movement can only occur through narrow 'gaps' at the junctions of endothelial cells. These gaps, approximately 100 Å wide, are estimated to occupy only 0·1 % of the total endothelial area. The necessity for the concentration of diffusion paths at these widely-spaced exit points underlines still further the importance of convection for assisting the transfer of slowly diffusing nutrients and metabolites to and from the tissues.

It is again the author's pleasure to acknowledge the encouragement and assistance of Professor M. J. Lighthill during the preparation of this work. The financial assistance of a Gowrie Travelling Scholarship is gratefully acknowledged.

Appendix A

Introduce the notation

$$\binom{RR}{ij} = \int_0^1 \frac{1}{r}\psi_i^R\psi_j^R\,dr, \qquad \binom{RI}{ij} = \int_0^1 \frac{1}{r}\psi_i^R\psi_j^I\,dr,$$

$$\binom{II}{ij} = \int_0^1 \frac{1}{r}\psi_i^I\psi_j^I\,dr, \qquad F_i^R = \int_0^1 \frac{1}{r}F_1\psi_i^R\,dr,$$

$$F_i^I = \int_0^1 \frac{1}{r}F_1\psi_i^I\,dr, \qquad G_i^R = \int_0^1 \frac{1}{r}G\psi_i^R\,dr,$$

$$G_i^I = \int_0^1 \frac{1}{r}G\psi_i^I\,dr.$$

Equations (2.20) may then be represented explicitly in matrix form as

$$\mathbf{S}.\mathbf{X} = \mathbf{D},$$

where
$$D_n = \begin{cases} F_n^R + a_n G_n^R - b_n G_n^I & (n = 1, \ldots, N), \\ F_{n-N}^I + a_{n-N} G_{n-N}^I - b_{n-N} G_{n-N}^R & (n = N+1, \ldots, 2N), \end{cases}$$

and
$$S_{ij} = (1 + a_i a_j)\binom{RR}{ij} - a_j b_i \binom{RI}{ji} - a_i b_j \binom{RI}{ij} + b_i b_j \binom{II}{ij},$$

$$-S_{i,j+N} = a_i b_j \binom{RR}{ij} - b_i b_j \binom{RI}{ji} + (1 + a_i a_j)\binom{RI}{ij} - a_j b_i \binom{II}{ij},$$

$$S_{i+N,j} = a_j b_i \binom{RR}{ij} + (1 + a_i a_j)\binom{RI}{ji} - b_i b_j \binom{RI}{ij} - a_i b_j \binom{II}{ij},$$

$$-S_{i+N,j+N} = b_i b_j \binom{RR}{ij} + a_i b_j \binom{RI}{ji} + a_j b_i \binom{RI}{ij} + (1 + a_i a_j)\binom{II}{ij},$$

for $i = 1, \ldots, N, j = 1, \ldots, N$. The solutions B_n^R, B_n^I are related to the solutions X_n by

$$B_n^R = X_n \quad (n = 1, \ldots, N),$$
$$B_n^I = X_{n+N} \quad (n = 1, \ldots, N).$$

Appendix B

Using the University of London CDC 6600 computer, with single precision accuracy to 14 significant figures, the eigenvalues α_n were obtained to 12 significant figures. Also the resulting eigenfunctions ψ_n, computed with a complex Bessel function routine accurate to 13 significant figures in the sector of interest, satisfied the boundary conditions (2.6) to 12 significant figures. The number of operations required to compute the integral coefficients defined in appendix A (using a 10-point Gaussian quadrature with successive halving of the interval) to 10-figure accuracy was of order 10^3; accuracy to at least 9 significant figures may then be expected for the matrix entries, and right-hand side vector, in the set of equations (2.20). Round-off errors here would lead to an error in the 11th place at worst and may be ignored.

Equations (2.20) were solved using Gaussian elimination with scaling, partial pivoting and iterative improvement of the initial results. For values of ϵ greater than about 0·001, precision to at least 12 significant figures were obtained in the initial (unimproved) solution. The condition of the matrix was therefore approximately of the order of 10^2, so that relative errors of 10^{-9} in the matrix entries and right-hand sides would lead to relative errors in the solution of order 10^{-7} at most. These are negligible compared with errors introduced by truncation of the series.

Sixty terms were used and, as might be expected, the condition that the radial velocity be zero at $z = \epsilon$ was satisfied to good accuracy, because of the absence of discontinuities of any kind in the function $G(r)$. On the other hand, the stream function boundary condition $F(r)$ has a discontinuity in the second derivative at the edge of the red-cell face. It might therefore be anticipated that convergence of the series expansion would be slow and that considerable errors would occur in matching the function $F(r)$. However, calculations showed that the coefficients of the dominant slowly decaying terms were obtained with excellent accuracy and were stable to variations in the level of trunction. Any errors in matching the boundary condition, therefore, decay extremely rapidly with decreasing z.

Appendix C

The equation for ψ_k can be written in the form

$$\frac{d}{dr}\left(\frac{1}{r}\frac{d\psi_k}{dr}\right)+\frac{\alpha_k^L}{r}\psi_k-\frac{\Psi_k}{r}=0, \tag{C 1}$$

where

$$\frac{d}{dr}\left(\frac{1}{r}\frac{d\Psi_k}{dr}\right)+\frac{\alpha_n^2}{r}\Psi_k=0.$$

Taking the real part of (C 1), we obtain

$$\frac{d}{dr}\left(\frac{1}{r}\frac{d\psi_k^R}{dr}\right)+\frac{\mathrm{Re}\,(\alpha_k^2)}{r}\psi_k^R-\frac{\mathrm{Im}\,(\alpha_k^2)}{r}\psi_k^I-\frac{\Psi_k^R}{r}=0=L_k(\psi_k^R,\psi_k^I),\text{ say.}$$

Using the equation

$$\psi_m^R L_n(\psi_n^R,\psi_n^I)-\psi_n^R L_m(\psi_m^R,\psi_m^I)=0,$$

we integrate to obtain, using the notation of appendix A,

$$[\mathrm{Re}\,(a_n^2)-\mathrm{Re}\,(\alpha_m^2)]\,(^{RR}_{nm}) = -\left[\frac{1}{r}\psi_m^R\frac{d\psi_n^R}{dr}-\frac{1}{r}\psi_n^R\frac{d\psi_m^R}{dr}\right]_0^1$$
$$+I_m(\alpha_n^2)\,(^{IR}_{nm})-I_m(\alpha_m^2)\,(^{RI}_{nm})+\int_0^1\frac{1}{r}(\Psi_n^R\psi_m^R-\Psi_m^R\psi_n^R)\,dr. \quad (C\ 2)$$

The first term on the right-hand side vanishes because of the boundary conditions satisfied by ψ_n, ψ_m. As n, m, $|n-m|$ become sufficiently large, $\mathrm{Re}\,(\alpha_n^2)\sim n^2$, $I_m(\alpha_n^2)\sim n\ln n$ and (C 2) becomes approximately

$$(^{RR}_{nm})\sim\frac{1}{n^2-m^2}\int_0^1\frac{1}{r}(\Psi_n^R\psi_m^R-\Psi_m^R\psi_n^R)\,dr.$$

This integral can similarly be reduced; two applications of the above procedure show that

$$(^{RR}_{nm})\sim\frac{A}{(nm)^{\frac{1}{2}}(n+m)(n^2-m^2)^2}.$$

Thus as n, m, $|n-m|$ increase, the matrix entries of the form

$$\int_0^1\frac{1}{r}\psi_n^R\psi_m^R\,dr$$

decrease rapidly to zero, as desired. Similar rationales may be devised for the other entries, with the same results.

REFERENCES

Aroesty, J. & Gross, J. F. 1970 *Microvascular Res.* **2**, 247.

Bloch, E. H. 1962 *Am. J. Anat.* **110**, 125.

Bloor, M. I. G. 1968 *Phys. Med. Biol.* **13**, 443.

Brånemark, P. I. & Lindström, J. 1963 *Biorheology*, **1**, 139.

Bugliarello, G. & Hsiao, G. C. 1970 *Biorheology*, **7**, 5.

Davidson, M. R. & Fitz-Gerald, J. M. 1972 *J. Fluid Mech.* (to appear).

Fitz-Gerald, J. M. 1969 *Proc. Roy. Soc.* B **174**, 193.

Fitz-Gerald, J. M. 1970 *J. Appl. Physiol.* **27**, 912.

Fitz-Gerald, J. M. 1972 In *Cardiovascular Fluid Dynamics* (ed. D. Bergel). Academic.

Guest, M. M., Bond, T. P., Cooper, R. G. & Derrick, J. R. 1963 *Science*, **142**, 1319.

Landis, E. M. & Pappenheimer, J. R. 1963 In *Handbook of Physiology*, p. 961. Washington: Am. Physiol. Soc.

Lee, H. S. & Fung, Y. C. 1969 *Biorheology*, **6**, 109.

Lee, H. S. & Fung, Y. C. 1970 *Biophys. J.* **10**, 80.

Lighthill, M. J. 1968 *J. Fluid Mech.* **34**, 113.

Lighthill, M. J. 1969 *CIBA Symposium on Circulatory and Respiratory Mass Transport*, p. 85. London: Churchill.

Luft, J. H. 1966 *Federation Proc.* **25**, 1773.

Palmer, A. A. 1959 *Quart. J. Expt. Physiol.* **44**, 149.

Prothero, J. W. & Burton, A. C. 1961 *Biophys. J.* **1**, 565.

Prothero, J. W. & Burton, A. C. 1962 *Biophys. J.* **2**, 199.

Scarton, H. A. 1970 Ph.D. thesis, Carnegie-Melton University, Pittsburgh.

Scarton, H. A. & Rouleau, W. T. 1971*a* (To be published.)

Scarton, H. A. & Rouleau, W. T. 1971*b* (To be published.)

Wang, H. & Skalak, R. 1969 *J. Fluid Mech.* **38**, 75.

Zidan, M. von 1969 *Rheologica Acta*, **8**, 89.